Shape-driven Segmentation of Intravascular Ultrasound Images

Gozde Unal[1], Susann Bucher[1], Stephane Carlier[2,3], Greg Slabaugh[1], Tong Fang[1], and Kaoru Tanaka[3]

[1] Siemens Corporate Research, Princeton, NJ, USA `gozde.unal@siemens.com`
[2] Department of Medicine-Cardiology, Columbia University, New York, USA
[3] Cardiovascular Research Foundation, New York, USA *

Abstract. Segmentation of arterial wall boundaries from intravascular images is an important problem for many applications in study of plaque characteristics, mechanical properties of the arterial wall, its 3D reconstruction, and its measurements such as lumen size, lumen radius, and wall radius. We present a shape-driven approach to segmentation of the arterial wall from intravascular ultrasound images in the rectangular domain. In a properly built shape space using training data, we constrain the lumen and media-adventitia contours to a smooth, closed geometry, which increases the segmentation quality without any tradeoff with a regularizer term. In addition, we utilize a non-parametric probability density based image energy, with global image measurements rather than pointwise measurements used in previous methods. This greatly enhances our segmentation method. The tests of our algorithm on a large dataset demonstrate the effectiveness of our approach.

1 Introduction

Intravascular ultrasound (IVUS) allows real time tomographic assessment of the arterial wall, which is very important for studying vascular wall architecture for diagnosis and assessment of the progression of the cardiovascular diseases [1]. Atherosclerosis is a disease characterized by a deposit of plaque in arterial wall over time. The disruption of an atherosclerotic plaque is considered to be the most frequent cause of heart attack and sudden cardiac death. Studying vulnerable plaques constitutes a major research area in the field of clinical and medical imaging. In order to track progression and regression during therapy of the atherosclerosis, the luminal and media/adventitial arterial wall is extracted and the plaque area is identified in the region between these two borders. Manual segmentation and processing is tedious, time-consuming, and susceptible to intra- and inter-observer variability. Due to the high number of images in a typical IVUS pullback, in the order of hundreds, automated segmentation of the arterial contours is an essential task.

Numerous approaches have been used to (semi-)automatically detect regions of interest in IVUS images. Most reported successful approaches are based on contour detection using a minimization of a cost function of the boundary contours or deformable models. Various optimization algorithms are applied. One approach is graph searching [2] in which prior knowledge of the expected IVUS pattern is incorporated. Other approaches are based on active contours [3, 4], probabilistic segmentation using elliptic templates [5], active contours

---

* We thank Sinan Biro and Celia Castellanos for their help in data collection and import.

through a neighborhood search [6, 7] and statistical distribution of blood and vessel wall tissue [8, 9].

None of the previous IVUS segmentation algorithms used a shape-driven approach, as we present in this paper. Medical IVUS image segmentation algorithms are almost always hampered by noise, stents, shadowing due to calcium deposits and have weak or missing boundaries of structures. Under such conditions, prior models proved to be useful in aiding the segmentation process. In fact, active shape models (ASMs) have become a popular tool in various segmentation applications for prostate, heart structures such as the left ventricle, and brain structures such as the corpus callosum [10–13]. The first ASMs [10] used parametric point distribution models learned through principal component analysis (PCA). The contours or shapes in a training dataset are first aligned to build an average shape, and eigen modes or eigenshapes obtained through PCA describe the variations from the mean shape. Implicit shape representations are now more popular since they solve the correspondence problem between shapes during the alignment stage [11, 12]. Our contribution in this paper is a shape-driven approach to IVUS segmentation. We will model both the lumen and medial/adventitial contour variations within a shape space, in the “resampled” rectangular domain. Hence, we constrain the lumen and media-adventitia contours to a smooth, closed geometry, which increases the segmentation quality without any tradeoff with a regularizer term, yet with adequate flexibility. In addition, we utilize a non-parametric probability density based image energy with global image measurements rather than pointwise measurements used in previous methods. This greatly enhances our segmentation method.

2 Shape Representation and Shape Space

In this paper, we build a statistical shape model to represent the inner and outer arterial wall contours in a compact way, and use this shape prior to drive the segmentation. The details of this method particular to the IVUS application are explained next.

2.1 2D Curves in “Re-sampled Rectangular” Domain

To build a statistical shape model, first a shape representation has to be selected. Typical lumen and medial/adventitial contours are shown in Figure 1 in both the display domain and the resampled rectangular domain, which is the original acquisition format. We choose the rectangular representation, since computations are much simpler due to the 1D appearance of the segmenting contours (see Figure 1b). Therefore, in the rectangular image domain $\Omega \in \mathbb{R}^2$, we utilize an implicit shape representation by embedding periodic contours $\boldsymbol{C} \in \Omega$ implicitly as the zero-level set of a signed distance function $\boldsymbol{\Phi} : \mathbb{R}^2 \longrightarrow \Omega$:

$$\boldsymbol{C} = \{(x, y) \in \Omega | \boldsymbol{\Phi}(x, y) = 0\}, \tag{1}$$

where $\boldsymbol{\Phi}(x, y) < 0$ is above (inside), and $\boldsymbol{\Phi}(x, y) > 0$ is below (outside) the contour.

2.2 Data Description

In-vivo pullbacks of 1529 frames on 20 patients were acquired with a Volcano Therapeutics Galaxy machine at 15 frames/sec with 1mm/sec using a 20MHz transducer. The pullbacks were taken from the left anterior descending artery (LAD), the right coronary arthery (RCA), and the left circumflex coronary artery (LCX). We used 257 frames to train our shape space and 1272 frames for testing. The patients used for training were not included in the testing.

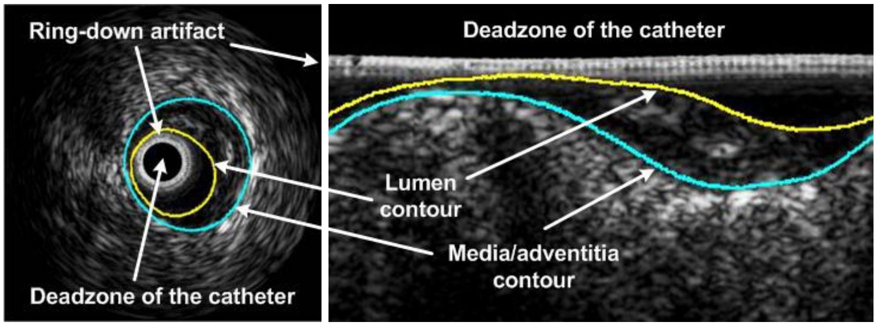

Display domain Rectangular domain

Fig. 1. Lumen and media/adventitia in display and rectangular domain.

The lumen and media/adventitia contours were segmented by an expert interventional cardiologist in our team, in order to provide the "ground truth" segmentation contours both for training and for testing.

2.3 Building a Shape Space

After the signed distance representations for the N lumen shapes $\boldsymbol{\Phi}^{\boldsymbol{l}}_{\boldsymbol{1}}, ..., \boldsymbol{\Phi}^{\boldsymbol{l}}_{\boldsymbol{N}}$, and media/adventitia shapes $\boldsymbol{\Phi}^{\boldsymbol{a}}_{\boldsymbol{1}}, ..., \boldsymbol{\Phi}^{\boldsymbol{a}}_{\boldsymbol{N}}$ in the training dataset are formed, we conduct statistical analysis. We align all the shapes radially by cropping them from the uppermost row (radial) coordinate where the contours can start, and the lowermost row coordinate where the media/adventitia contours can end. The horizontal (angular) shift of the shape in the rectangular grid corresponds to a rotation of the shape in the display domain. We have not carried out an alignment in the horizontal direction because we would like the shape space to capture those shifts through its eigenshapes.

We compute the mean lumen shape: $\boldsymbol{\Phi}^{\boldsymbol{l}}_{\mathbf{mean}} = \frac{\boldsymbol{1}}{\boldsymbol{N}} \sum_{\boldsymbol{i=1}}^{\boldsymbol{N}} \boldsymbol{\Phi}^{\boldsymbol{l}}_{\boldsymbol{i}}$, and the mean medial/adventitial shape:$\boldsymbol{\Phi}^{\boldsymbol{a}}_{\mathbf{mean}} = \frac{1}{N} \sum_{i=1}^{N} \boldsymbol{\Phi}^{\boldsymbol{a}}_{\boldsymbol{i}}$. We subtract them from each shape in the training set to construct the shape variability matrices $\boldsymbol{S}^{\boldsymbol{l}} = [\tilde{\boldsymbol{\Phi}}^{\boldsymbol{l}}_{\boldsymbol{1}} \cdots \tilde{\boldsymbol{\Phi}}^{\boldsymbol{l}}_{\boldsymbol{N}}]$ and $\boldsymbol{S}^{\boldsymbol{a}} = [\tilde{\boldsymbol{\Phi}}^{\boldsymbol{a}}_{\boldsymbol{1}} \cdots \tilde{\boldsymbol{\Phi}}^{\boldsymbol{a}}_{\boldsymbol{N}}]$. After PCA is carried out on both $\boldsymbol{S}^{\boldsymbol{l}}$ and $\boldsymbol{S}^{\boldsymbol{a}}$, we obtain our models that represent each shape as variations around the mean:

$$\boldsymbol{\Phi}^{\boldsymbol{l}}(w) = \boldsymbol{\Phi}^{\boldsymbol{l}}_{\mathbf{mean}} + \sum_{i=1}^{k} w^l_i \boldsymbol{U}^{\boldsymbol{l}}_{\boldsymbol{i}} \tag{2}$$

where $w^l = \{w^l_1, w^l_2, ..., w^l_k\}$ are the weights associated with the first k principal modes $\boldsymbol{U}^{\boldsymbol{l}}_{\boldsymbol{i}}$. The same analysis is carried out for the training set containing the media/adventitia shapes.

In Figure 2, the eigenshapes representing the first four variations in the lumen shape space are shown by varying them around the luminal mean shape: $\boldsymbol{\Phi}^{\boldsymbol{l}}_{\mathbf{mean}} + w^l_i \boldsymbol{U}^{\boldsymbol{l}}_{\boldsymbol{i}}$, with i = {1, 2, 3, 4}. Note that the first mode deformation corresponds to a negative/positive amplification of the curving, the second mode to a radial shift (distance to the catheter and change of the lumen area) although it also includes an angular shift effect. The third mode corresponds to a flattening vs. curving whereas the fourth and higher modes explain more local variations of the shape. The same interpretations can be made for the eigenshapes of the media/adventitia contours. As we can see from Figure 2 the arterial wall contours form a fairly restricted class of shapes, therefore a small number of eigenshapes $\{\boldsymbol{U}^{\boldsymbol{l}}_{\boldsymbol{i}}\}_{i=1}^{k}$ and $\{\boldsymbol{U}^{\boldsymbol{a}}_{\boldsymbol{i}}\}_{i=1}^{k}$ is needed to explain

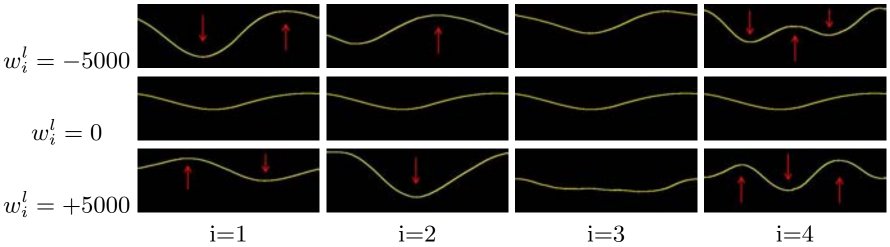

Fig. 2. Luminal mean shape with weight variations for the first four modes.

its variations. In our experiments we found that six principal modes suffice for lumen and media/adventitia, respectively, to obtain shapes that are both meaningful and smooth.

3 Segmentation Framework

Once we build the statistical shape space, any arterial wall can be represented by a vector of weights $w_1^l, ...w_k^l$ associated with the first k principal modes of the lumen data, and $w_1^a, ...w_k^a$ of the media/adventitia data. The weights of any shape can be found using Eq. (2) by projecting the shape matrix without the mean onto the mode matrix:

$$\boldsymbol{w}^{\,l} = \boldsymbol{U}_{\,l}^{\,T}\ (\boldsymbol{\Phi}^{\,l} - \boldsymbol{\Phi}^{\,l}_{\text{mean}}) \qquad (3)$$

where $\boldsymbol{\Phi}^{\,l}$ represents the truncated mode matrix in the reduced subspace. With this compact shape description, we will evolve the shape weights $\boldsymbol{w}$ directly to deform the contour towards the lumen and media/adventitia borders in the IVUS image. The steps of the segmentation are explained next.

3.1 Preprocessing

In IVUS images, the catheter creates a dead zone in the center of the display domain, or the top rows of the rectangular domain, along with the imaging artifacts due to "halo" ring-down effects of the catheter (see Figure 1). These regions need to be removed because otherwise they will hamper the segmentation process. The standard approach, that is to subtract the average image from every frame, does not remove the artifact properly and degrades the image quality. For our data we observe that the artifact stays approximately constant over the IVUS sequence of frames. However, the variance of the artifact is not zero because the luminal border often interferes with the artifact zone. By taking the minimum image $I_{\text{min}}(x, y) = \min_{i\in\lambda} I_i(x, y)$ over a set of frames I_i of the IVUS sequence λ (e.g. 20 frames), we get the constant artifact zone without the bright interferences with the contour. We compute the sums over the rows of I_{min} and find the global maxima. The catheter artefact is noted down as the row at which the row sum falls below 50%. We omit the rows above this artifact line from any kind of computations involved in our segmentation. The first local minimum after the global maximum indicates us the end of the artifact. We subtract the artifact zone of I_{min} from every frame, as shown in Figure 3a and b.

3.2 Lumen Segmentation

The next step is to initialize the lumen contour in a way that takes advantage of the prior information about the lumen region having less ultrasound reflection, hence a dark intensity profile. We shift the mean lumen shape $\boldsymbol{\Phi^l_{\text{mean}}}$

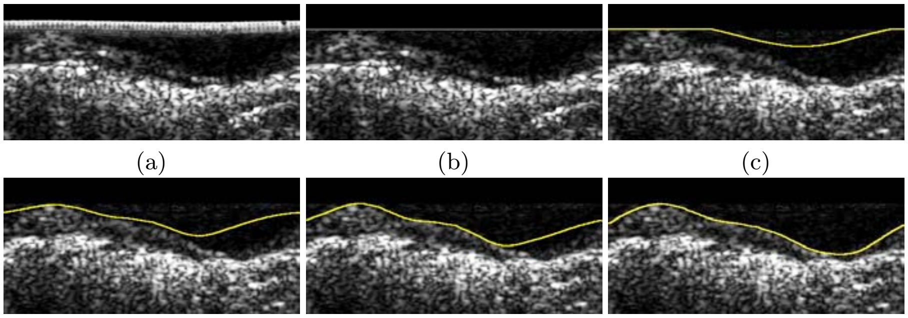

(a) (b) (c)

(d) (e) (f)

Fig. 3. (a)-(b) Rectangular domain before and after artifact removal, (c) initialization of the luminal contour and (d)-(f) evolution of the luminal contour after 3,6 and 9 iterations.

in angular direction to minimize the mean intensity above the contour. This simple strategy for the initial shape pose works well as shown in Figure 3c.

For the evolution of the luminal contour we utilize region statistics from IVUS images for segmentation, and define the following energy

$$E_{\text{lumen}}(\boldsymbol{w}^{l}) = \int_{\Omega} -\mathcal{X}_{in}(\boldsymbol{x}) \log(P_{in}(I(\boldsymbol{x}))d\boldsymbol{x} + \int_{\Omega} \mathcal{X}_{out}(\boldsymbol{x}) \log(P_{out}(I(\boldsymbol{x}))d\boldsymbol{x} \tag{4}$$

where $\mathcal{X}$ is an indicator function for inside and outside the contour. This is the familiar regional probabilistic energy [13]. To estimate the probability distributions P_{in} and P_{out}, we use the Kernel density estimator: $P(q) = \frac{1}{N\sigma}\sum_{i=1}^{N} K(\frac{q-q_i}{\sigma})$, where N is the number of pixels inside or outside the contour and $K(p) = \frac{1}{\sqrt{2\pi}} exp(-\frac{p^2}{2})$, with a heuristically chosen σ value (e.g. $\sigma = 10$).

Finally, we take the first variation of the energy in Equation (4) to find the gradient flow of the contours represented by the weight vector $\boldsymbol{w}$. The Euler-Lagrange equations result in the ordinary differential equation (ODE):

$$\frac{\partial w_i^l}{\partial t} = \int_{\boldsymbol{C}} -\log(P_{in}(I(\boldsymbol{x}))/P_{out}(I(\boldsymbol{x}))\boldsymbol{U}_i^l d\boldsymbol{x}\,, \tag{5}$$

where $\boldsymbol{U}_i^l$ is the corresponding eigenshape.

The equation above uses pointwise intensity measurements on the contour, therefore may be hampered by speckle noise in the lumen. We design a more global intensity term I_{modified} that avoids the contour getting stuck in local minima. This intensity utilizes a maximum function of the averaged intensity over the column above the contour position $\boldsymbol{x} = (x, y)$:

$$I_{\text{modified}}(x, y) = \max_{y_0 \in [0,y]} \frac{1}{y - y_0 + 1} \sum_{y_i = y_0}^{y} I(x, y_i), \tag{6}$$

where the origin of the image (0,0) is in the top left corner. We then replace $I(\boldsymbol{x})$ in Equation (5) with $I_{\text{modified}}(\boldsymbol{x})$.

We constrain the luminal contour by the artifact line (see Figure 3b). The evolution of the shape weights, hence the segmentation, over the artificial evolution time t is depicted in Figure 3c- 3f.

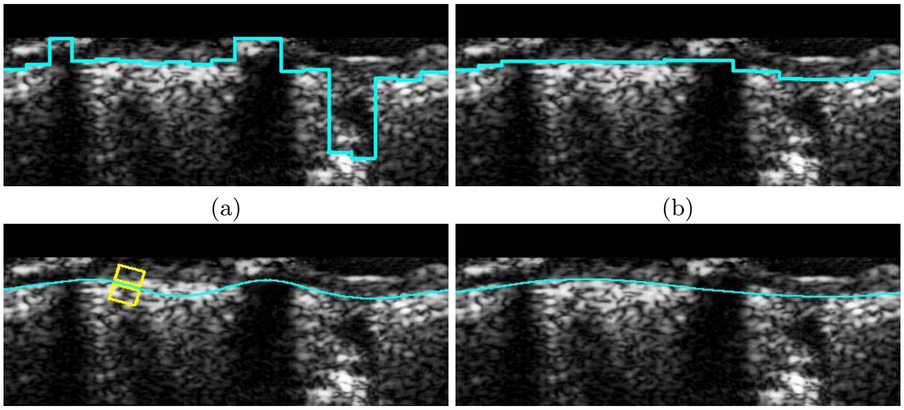
(a) (b) (c) (d)

Fig. 4. Segmentation of media/adventitia: (a) max intensities contour (b) median filtered contour (c) initial shape pose with gradient window (d) evolved contour (after six iterations)

3.3 Media/adventitia Segmentation

In IVUS images, the media is observed as a thin black line, whereas the adventitia tissue has echogenic characteristics and appears very bright. We take advantage of this anatomical observation by employing edge information. However, a pointwise gradient is not very useful because of the noise present in IVUS images. We define a smoother version of the gradient as the difference between the average intensity of a square above and below the current pixel position.

For the initialization of the media/adventita contour we divide the rectangular image into 25 columns (= 14.4° angular intervals). We find the position of maximal gradient for every column. This will give us a first initialization of the media/adventitia contour (see Figure 4a). A median filter (of size 7) that is passed over this initial contour eliminates eventual noise due to small artifacts or openings as shown in Figure 4b. We use the median filtered contour to obtain our initial shape pose (see Figure 4c).

For the evolution of the media/adventitia contour we compute the gradient as the difference between the average intensity of two oriented windows above and below the contour as shown in Figure 4c. We utilize the familiar edge-based energy [14], and derive the ordinary differential equation (ODE) for the media/adventitia contour, with ∇G representing the smoothed oriented edge gradient:

$$\frac{\partial w_i^a}{\partial t} = \int_{\boldsymbol{C}} \nabla G(\boldsymbol{x}\,)\boldsymbol{U}\,_i^a d\boldsymbol{x}\;. \tag{7}$$

In addition, we incorporate an anatomical constraint to the evolution of the media/adventita so that the minimum distance to the lumen is 0.2mm.

4 Results and Discussions

We tested our IVUS segmentation algorithm on 1272 images from IVUS pullbacks of 18 different patients. The update equations (5) and (7) are used to segment the lumen and media/adventitia contours and they typically converge after 5 to 50 iterations. Figure 5 demonstrates our results for several frames. We found that our media-adventitia algorithm works very well when there are no

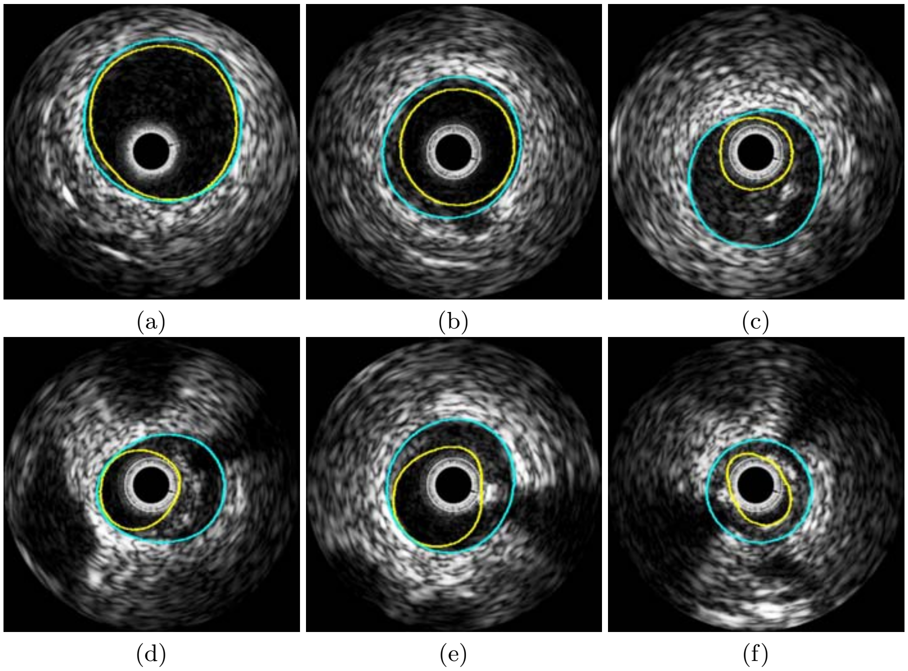
(a) (b) (c)
(d) (e) (f)

Fig. 5. Six examples of automatically computed lumen and media/adventitia contours, including the cases of (a) healthy artery without plaque (b) centric catheter (c) small lumen with spurious noise between lumen and media/adventitia (d)-(f) calcification with black shadow

very strong features such as a large calcification or a large side branch opening. With minor calcification and side branches, the segmentation is fairly successful due to the nicely constrained shape space in which our segmentation takes place. Because of this, even if there are openings, noise or other artifacts, the contour stays as a closed smooth contour, and can achieve meaningful results. Table. 1 depicts the percentage of true positive pixels, false positive pixels, and absolute area differences. It can be observed that our algorithm achieved a 96.99% correct classification for the lumen contour, and a 92.74% for the media-adventitia contour.

Table 1. Percentage of true positive and false positive pixels, and the absolute area differences between the segmentation maps of our algorithm and the physician's manual delineations for both the lumen and the media/adventitia contours, averaged over 1272 IVUS frames.

	True Positives (%)	False Positives (%)	Absolute Area Difference (mm^2)
Lumen Contours	96.99 ± 32.30	11.14 ± 8.41	0.677 ± 0.617
M-A Contours	92.74 ± 7.75	3.30 ± 4.95	0.719 ± 0.914

The pixel size is 25 x 25 μm^2.

With a 20MHz IVUS probe, it can be observed that a fair amount of speckle noise is present in the lumen. However, a higher frequency probe (40MHz) will produce more speckle noise. Therefore, the lumen segmentation has to be adopted by computing a new intensity probability distribution. This will be part of our future studies.

5 Conclusion

We have presented a shape-driven approach for segmenting arterial wall from IVUS images in the “resampled” rectangular domain. Our experiments demonstrate that this method can be used in plaque analysis, 3D reconstruction of the arterial wall and for measurements such as lumen size, lumen radius, wall radius, and so on. In future work we plan to focus on detecting calcifications and branch openings, and incorporating that knowledge into the medial/adventitial contour extraction. We will also take advantage of the continuity of images in the IVUS pullback sequences and enhance our algorithm by extending it to 3D.

References

1. Nissen, S., Yock, P.: Intravascular ultrasound: Novel pathophysiological insights and current clinical applications. Circulation **103** (2001) 604–616
2. Sonka, M., Zhang, X., Siebes, M., Bissing, M., DeJong, S., Collins, S., McKay, C.: Segmentation of intravascular ultrasound images: A knowledge-based approach. IEEE Trans. on Medical Imaging **14**(4) (1995) 719–732
3. Kovalski, G., Beyar, R., Shofti, R., Azhari, H.: Three-dimensional automatic quantitative analysis of intravascular ultrasound images. Ultrasound Med Biol. (26) (2000) 527–537
4. Dijkstra, J., Koning, G., Tuinenburg, J., Oemrawsingh, P., Reiber, J.: Automatic border detection in intra vascular ultrasound images for quantitative measurements of the vessel, lumen and stent parameters. In: Computers in Cardiology. (2001) 25–28
5. Gil, D., Radeva, P., Saludes, J.: Segmentation of artery wall in coronary ivus images: A probabilistic approach. In: IEEE Int. Conf. on Pattern Recognition. (2000)
6. Klingensmith, J., Shekhar, R., Vince, D.: Evaluation of three-dimensional segmentation algorithms for the identification of luminal and medial-adventitial borders in intravascular ultrasound images. IEEE TMI **19**(10) (2000) 996–1011
7. Plissiti, M., Fotidadis, D., Michalis, L., Bozios, G.: An automated method for lumen and media-adventitia border detection in a sequence of ivus frames. IEEE Trans. on Information Technology in Biomed. **19**(10) (2000) 996–1011
8. Brusseau, E., deKorte, C., Mastik, F., Schaar, J., van der Steen, A.: Fully automatic luminal contour segmentation in intracoronary ultrasound imaging- a statistical approach. IEEE Trans. on Medical Imaging **23**(5) (2004) 554–566
9. Cardinal, M.H., Meunier, J., Soulez, G., Maurice, R., Therasse, E., Cloutier, G.: Automatic 3d segmentation of intravascular ultrasound images using region and contour information. In: MICCAI. Volume LNCS-3749. (2005) 319–326
10. T.F Cootes, C.J Taylor, D.C., Graham, J.: Active shape models - their training and application. Computer Vision and Image Understanding **61**(1) (1995) 38–59
11. Leventon, M., Grimson, W., Faugeras, O.: Statistical shape influence in geodesic in active contours. In: Proc. CVPR. (2000) 316–323
12. Tsai, A., Yezzi, A., Wells, W., Tempany, C., Tucker, D., Fan, A., Grimson, W., Willsky, A.: A shape-based approach to the segmentation of medical imagery using level sets. IEEE Trans. on Medical Imaging **22**(2) (2003) 137–154
13. Rousson, M., Cremers, D.: Efficient kernel density estimation of shape and intensity priors for level set segmentation. In: MICCAI. (2005) 757–764
14. Kichenassamy, S., Kumar, A., Olver, P., Tannenbaum, A., Yezzi, A.: Gradient flows and geometric active contours. In: Proc. ICCV. (1995) 810–815